



Effects of Excess Air and Energy Fraction on Heat Transfer for Co-firing of Eucalyptus Bark and Peanut Shell Blended Fuel in a Twin-Cyclonic Swirling Fluidized-Bed Combustor

Kasama Sirisomboon¹ · Nattawat Sopamart^{1,2} · Tananon Srisamran³

Received: 29 July 2023 / Revised: 14 October 2023 / Accepted: 19 October 2023 / Published online: 15 February 2024
© The Author(s), under exclusive licence to Korean Institute of Chemical Engineers, Seoul, Korea 2024

Abstract

Biomass plays an important role in mitigating greenhouse gas (GHG) emissions. However, the major problem in using biomass is that inconsistent amounts are available throughout the year. The use of mixed fuels is one way to solve this problem. Based on the lumped system analysis method, this experimental study investigated the effects of excess air (*EA*) and energy fraction on the heat transfer coefficients of co-firing eucalyptus bark and peanut shell in a twin-cyclonic swirling fluidized-bed combustor. The blended fuel was fired at a fixed heat rate for various energy fractions of secondary fuel (EF_2) and *EA*. The radial and axial heat transfer coefficients were observed: the average heat transfer coefficient of each operating condition showed significant effects for *EA*, while the effect for EF_2 was not obvious. The heat transfer coefficient could be improved by up to 11% in the bed region and by as much as 22% in the freeboard area when *EA* was increased from 40–80%.

Keywords Biomass combustion · Heat transfer coefficient · Lumped system analysis · Local heat transfer · Swirling fluidized-bed combustor

Abbreviations

List of symbols

A_S	Lumped surface area (m ²)
A_Z	Cross-sectional area of combustor at level Z (m ²)
Bi	Biot number
$C_{p,lump}$	Specific heat of lumped area (J/kg K)
d_i	Inner diameter (m)
d_o	Outer diameter (m)
d_p	Mean bed particle diameter (m)
<i>EA</i>	Excess air
EF_2	Energy fraction of secondary fuel

<i>FR</i>	Fuel feed rate, kg/h
h_{avg}	Average heat transfer coefficient (W/m ² K)
h_{local}	Local heat transfer coefficient at the investigating point (W/m ² K)
$h_{z,avg}$	Average heat transfer coefficient at level Z (W/m ² K)
MF_2	Mass fraction of secondary fuel
m_{lump}	Mass of lumped area (kg)
r/R	Radial direction
t	Time duration during the temperature measurement (s)
T_{ini}	Initial temperature of lumped area (K)
T_{lump}	Temperature of lumped surface at every second (K)
T_m	Mean temperature of fluidizing gas (K)
v_p	Primary air velocity (m/s)
V	Volume of the combustor (m ³)

Greek symbols

ρ_p	Density of solid (kg/m ³)
V^0	Theoretically required volume of air, m ³ /kg fuel

Subscripts

1	Primary
2	Secondary
g	Gas

✉ Kasama Sirisomboon
sirisomboon_k@su.ac.th

¹ Laboratory of Advanced Combustion Technology and Energy Systems, Department of Mechanical Engineering, Faculty of Engineering and Industrial Technology, Silpakorn University, Nakhon Pathom 73000, Thailand

² Gulf TS2 Company Limited, 545 Moo1 Eastern Seaboard Industrial Estate (Rayong) Tasit, Pluak Deang, Rayong 21140, Thailand

³ Office of the Permanent Secretary, Ministry of Energy, Kanchanaburi City Hall, Kanchanaburi 71000, Thailand

i	Inner
ini	Initial
m	Mass
o	Outer
p	Primary air
s	Surface
Z	Height above the air distributor

Introduction

With the European Environment Agency's 2030 *Climate Target Plan's* aim of cutting greenhouse gas (GHG) emissions by at least 55% of 1990 levels [1], biomass fuel has been promoted as the CO₂ neutral fuel for power plants. Its usage has significantly increased over the past few years due to the energy policy supported by many countries' governments [2, 3]. Even though biomass has an abundant supply of resources, almost all biomass fuel is periodically obtained from agricultural harvesting and as a by-product of manufacturing processes, such as those in the wood industry, furniture manufacturing industry, paper mill industry, and the sugar industry. Therefore, it is not possible to ensure the supply of a consistent amount throughout the year. To achieve stable power output, fuel comprised of mixed biomass sources, such as wood and straw, wheat straw and pine, stem wood and softwood bark, cassava rhizome and eucalyptus bark (EB), peanut and tamarind shells, has been introduced and utilized in many power plants [4–7]. This technique is intended to not only overcome the fuel supply problem, but also to minimize emissions and reduce slagging and fouling propensities [5, 8, 9].

In Thailand, eucalyptus is widely grown in commercial plantations to produce raw materials for the pulp and paper industry. This plant can be grown in all weathers in any area even if planted in poor soil. In 2020, Thailand's Department of Agriculture Extension [10] reported the EB growth area as being 737,882 *rai* (*rai* is the Thai unit of area), equivalent to 1,180.6 square kilometers (km²). Compared to other hardwood forest biomass, eucalyptus has quite a short rotation coppice of about 4–7 years. With the advantages of a high gross calorific value of 17.1 MJ/kg [11] and the availability of this kind of feedstock, EB is an outstanding choice for a biomass power plant.

An excellent plant-based source of protein, vitamins, minerals, and antioxidants, groundnuts or peanuts are one of the most common types of nuts consumed. In 2020, as consumption of plant-based food continued to boom, the world production of peanuts (reported as groundnuts in shells) increased by about 8% to reach a market volume of 54 million tons [12]. Thailand's domestic demand for peanuts reached 113,498 tons in 2021 [13]. After harvesting, drying, cleaning, and screen sizing, peanuts are introduced

to the crushing process, of which peanut shells (PNS) are the by-product [14]. PNS are dried, easy to accumulate, and quite uniform in size. They also have quite a high calorific value of 16.78 MJ/kg [15] and, thus, can be considered as potential fuel for heat and power generation.

Due to the many advantages of the fluidized-bed combustor (FBC), such as the uniform combustion temperature, high combustion efficiency (above 98%) [6, 16], and quite low emissions, the FBC system is the most commonly used system in new age power plants [17]. Among the famous types of the FBC system, including bubbling fluidized-bed and circulating fluidized-bed systems, the swirling fluidized-bed system is regarded as the most attractive technique. It provides a long residence time and good mixing of fuel-bed material, consequently producing excellent combustion at quite a low temperature [18, 19]. Moreover, at the optimum excess air (*EA*) and controlling combustor load, this combustor can also achieve very low emissions of nitrous oxides (NO_x) [16].

The utilization of heat production from the FBC process is the greatest challenge in an engineering work as it involves heat transfer between two-phase flows of gas–solid (fuel, ash, and bed material) and the heat transfer surface where the erosion/corrosion takes place [20]. Moreover, the mechanisms of heat transfer in different regimes, for example, dense bed, bed splash zone, and freeboard region, of the FBC are complicated. In fluidization, the heat transfer coefficient can be described by three mechanisms: particle convection, gas convection, and radiation. In the bed region, the dense clusters of particles enhance contact time between the bed particles and the immersed surface, ultimately increasing the particle convection heat transfer [21–24]. Good mixing between bed particles and fluidizing air, with an appropriate amount of primary and secondary air, thus leads to a higher heat transfer coefficient. In our previous study, the highest heat transfer coefficient occurred in the bed area. In the freeboard region, the heat transfer coefficient was about 12% lower than in the bed region [25]. The gas convection mechanism dominated due to dilution of the bed material. Therefore, the effects of the operating velocity were more sensitive in this area, especially with fine bed particles [21].

From many studies in the literature on heat transfer during the combustion of solid fuel in the FBC, it can be concluded that the heat transfer coefficient is dominated by: (1) fluidization type; (2) operating conditions: fuel feed rate, *EA*, and ratio of primary and secondary air injection; (3) type and particle size of inert bed material; and (4) combustor's design feature: shape of the combustor and air distributor system [21, 25].

Compared to research on heat transfer in bubbling and circulating fluidizations, knowledge from investigations of heat transfer in the swirling FBC is quite limited, even under the cold test condition. Therefore, to better understand heat

transfer in the swirling FBC, this experimental study aimed to study the co-firing of the blended fuel of EB and peanut shell (PNS) in a twin-cyclonic swirling fluidized-bed combustor (TS-FBC). The study's main focus was the effects of the mass/energy fractions of EB and PNS on the fuel mixture, while also exploring the effects of the operating condition [i.e., excess air (*EA*)] on the heat transfer coefficient.

Materials and Methods

Experimental Setup

A TS-FBC was used in the co-firing tests (and is shown with its equipment in Fig. 1). The combustor consisted of two cyclonic-shaped combustors assembled with a 0.25-m inner diameter circular pipe along the vertical axis. Each cyclonic-shaped combustor had a 40° conical section with a 0.25-m inner diameter at the bottom and a 0.7-m inner diameter at the top. The conical and cylindrical sections had a total height of 1.2 m, while the TS-FBC had a total height of 2.8 m. To avoid heat loss due to radiation and convection from the combustor surface area, the combustor's inner wall was insulated with 0.1 m of refractory cement. The current study used an air distributor with the swirling number of 2.76.

A 10-hp forced draft blower with a variable speed control device supplied fluidizing air at the specific range of the *EA* ratio. The biomass fuels were fed into the TS-FBC at a height of 0.95 m above the air distributor by the screw-type feeder. The flue gas treatment system consisted of a cyclone separator and a wet scrubber. To verify the *EA*, the

concentrations in flue gas of oxygen (O_2), carbon monoxide (CO), and hydrocarbon (C_xH_y , as CH_4) were sampled.

To observe the radial and axial heat transfer coefficients along the combustor, five sampling ports were installed at different levels along the combustor, as shown in Fig. 1. To investigate combustion behavior inside the combustor, six stationary thermocouples of type K (± 2.2 °C accuracy) were employed along the height of the combustor.

Fuels and Bed Material

The fuels for the co-firing tests were collected as by-products from different industries. EB was obtained from the pulp and paper industry, while peanut shell (PNS) was delivered from the peanut shelling plant. The EB was shredded due to its non-uniform shape and size before it was supplied to the combustor. Following that process, the individual EB fibers were still quite irregular, ranging from 0.1 mm to about 10 mm in length; however, this would not cause the screw-type feeder any problems. The average solid bulk densities of the shredded EB and PNS were 73.76 kg/m^3 and 180.07 kg/m^3 , respectively. The proximate and ultimate analyses on an as-received basis, along with the lower heating value (LHV), are shown in Table 1. As can be seen, the LHV of the EB was slightly lower than that of the PNS due to its high fuel moisture content ($W = 14.55\%$).

To sustain the mixed fuel's uniformity, the PNS and the EB were blended together before being supplied to the combustor. In the current study, the EB was the primary fuel, while the PNS was the secondary fuel. The mass fraction of the secondary fuel (MF_2) was calculated by Eq. (1), while

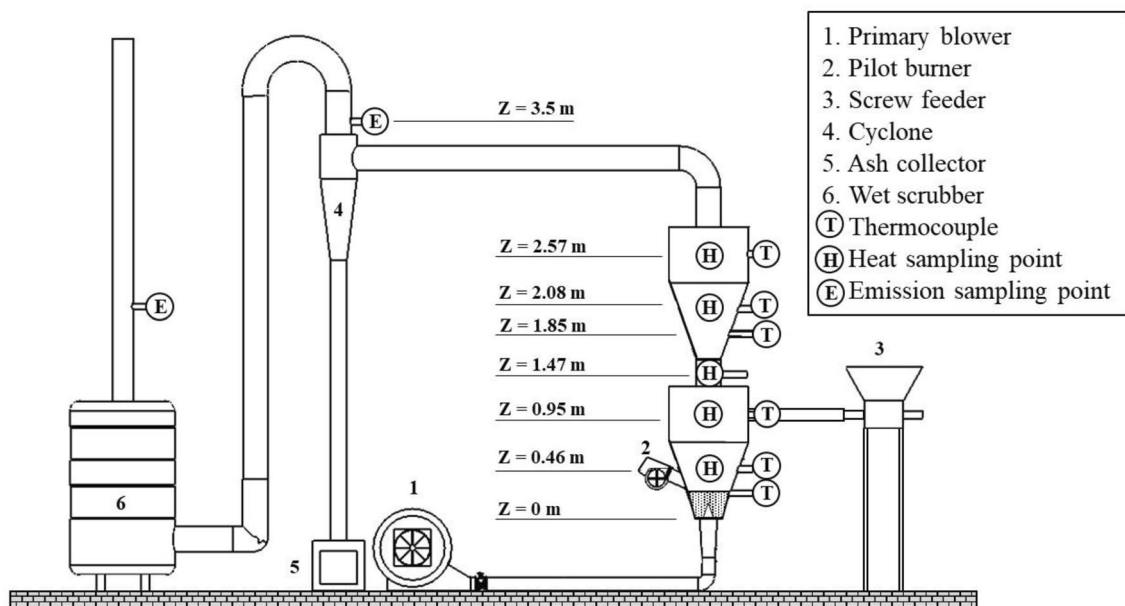


Fig. 1 Schematic diagram of a TS-FBC

Table 1 Properties of EB and PNS used in experimental tests

Fuel	Ultimate analysis basis (wt%, as-received basis)					Proximate analysis basis (wt%, as-received basis)				LHV (kJ/kg)
	C	H	N	O	S	W	A	VM	FC	
EB	32.87	4.91	0.04	39.23	0.0	14.55	8.4	60.89	14.73	11,608
PNS	36.1	4.99	0.36	35.87	0.04	7.72	14.91	61.86	14.26	13,325

A fuel ash, C carbon, FC fixed carbon, H hydrogen, LHV lower heating value, N nitrogen, O oxygen, S sulfur, VM volatile matter, W fuel moisture

the energy fraction of the secondary fuel (EF_2) was calculated based on the LHV of each fuel and MF_2 as can be seen in Eq. (2). During the co-firing tests, MF_2 was varied with four fuel options of 0, 0.28, 0.53, and 0.77 energy fractions, with the fuel feed rate of each fuel shown in Table 2. To sustain the same heat release rate of the blended fuel at 72.5 kW_{th}, the total feed rate for each test was varied as can be seen in Table 2

$$MF_2 = \frac{FR_2}{FR_1 + FR_2} \quad (1)$$

$$EF_2 = \frac{MF_2(LHV_2)}{(1 - MF_2)LHV_1 + (MF_2)LHV_2} \quad (2)$$

In line with studies from the literature review, the current study selected sand comprising Geldart's type-B particles to be the inert bed material [23, 26, 27]. The bed material had a solid density of 1650 kg/m³ with the particle-size diameter ranged from 450 to 550 μm. The static bed height was fixed at 30 cm for all tests. At the completion of each test, the bed material was observed for agglomeration. Every 60–80 h of usage, the bed material was changed to avoid bed agglomeration problems.

Measurement of Heat Transfer Coefficient

Lumped system analysis is one of the simplest ways to analyze heat transfer. It was introduced by Wang et al. [28] and Sjösten et al. [29] to investigate the heat transfer coefficient in the fluidized-bed system. For the lumped capacitance model, the shape and size of the sampling material are not

counted as long as the Biot number (Bi) of the heat transfer sampling material is less than 0.01 [29, 30]. For the current study, a copper rod 9 mm in diameter and 25 mm in length was used as the lumped material. The properties of the copper rod were 8,933 kg/m³ for density; 385 J/kg K for specific heat capacity ($C_{p,lump}$); 7.24×10^{-6} m³ for volume (V); and 9.03×10^{-4} m² for surface area (A_s), respectively. The Bi was calculated from these properties and was less than 0.01. By employing the resolution of a data logger, the accuracy of temperature measurement, and the fluctuation of data with the approach emphasized by Holman [31], an uncertainty analysis in this experimental study is $\pm 17\%$.

The heat transfer probe is shown in Fig. 2. As can be seen, seven copper rods were installed at radial directions of $r/R = 0, \pm 1/3, \pm 2/3$, and ± 1 . Three different lengths of heat transfer probes were required to measure the heat transfer coefficient for the five levels along the combustor which had three cross-sectional areas at the conical section, cylindrical section, and connecting pipe. These lengths were 500 mm for the conical section, 700 mm for the cylindrical section, and 200 mm for the connecting pipe. The details of the sampling material and the probe were as described by Sirisomboon and Laowthong [25]. For the investigation of heat transfer in the bed and freeboard regions, the five levels for measuring heat transfer were at $Z = 0.46$ m, 0.95 m, 1.47 m, and 2.08 m above the air distribution system as seen in Fig. 1.

During the experimental tests, the heat transfer coefficients were investigated under the steady-state condition. The temperatures of the sampling rods of the heat transfer probes were recorded for 30 s, with the probes then removed to avoid sandblasting and cracking due to high temperature.

Table 2 Proportion of blended fuel of eucalyptus bark (EB) and peanut shells (PNS) used in co-firing tests

Mass fraction of secondary fuel (MF_2)	Energy fraction of secondary fuel (EF_2)	Feed rate (kg/h)		Total fuel feed rate (kg/h)
		Eucalyptus bark	Peanut shells	
0	0	22.5	0	22.5
0.25	0.28	16.88	4.9	21.78
0.5	0.53	11.25	9.8	21.05
0.75	0.77	5.63	14.7	20.33
1	1	0	19.6	19.6

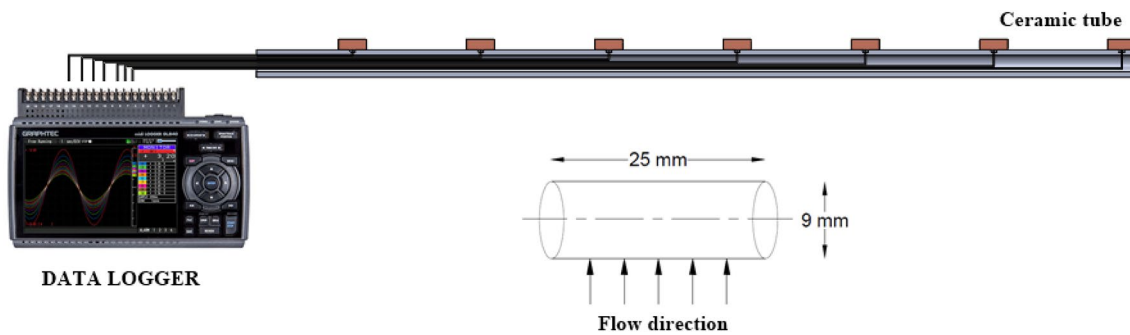


Fig. 2 Heat transfer probe used in the experimental tests

In a more detailed analysis, the heat transfer coefficients in this study were characterized by: (1) local heat transfer (h_{local}); (2) average heat transfer at each combustor height ($h_{z,\text{avg}}$); and (3) average heat transfer coefficient for each operating condition (h_{avg}). The h_{local} was derived by lumped system analysis as shown in Eq. (3)

$$h_{\text{local}} = -\left(\frac{m_{\text{lump}}c_{p,\text{lump}}}{A_s}\right) \times \frac{\ln\left(\frac{T_{\text{lump}}-T_m}{T_{\text{ini}}-T_m}\right)}{t}. \quad (3)$$

The $h_{z,\text{avg}}$ was calculated from the seven h_{local} for each specific height by Eq. (4), as suggested by Sun et al. [32] and Sirisomboon and Laowthong [25]

$$h_{z,\text{avg}} = \frac{1}{A_z} \int h_{\text{local},i} dA_{z_i}. \quad (4)$$

The h_{av} was calculated from the five values of $h_{z,\text{avg}}$ along the combustor height at Z_1 – Z_5 as provided below

$$h_{\text{avg}} = \frac{1}{V} \int_{Z_i}^{Z_{i+1}} h_{z_i,\text{avg}} dV_{z_i}. \quad (5)$$

Experimental Test Planning

Before the mixed biomass was utilized in the co-firing tests, the EA was appropriately adjusted to achieve Thailand's emissions standard set by Thailand's Pollution Control Department [33]. As mentioned above, the EB had a wide range of particle sizes ranging from the very fine to coarse particles. Therefore, preliminary tests were required for the different EA values. To fire the mixed fuel at 20% EA , the CO and NO_x emissions were investigated, with the value of CO emissions found to exceed the emissions restriction standard. From the temperature and flame investigation, it could be concluded that the EB's coarse particles were vigorously burned in the main combustion, while the fine particles flew up and fired in the upper

chamber. Due to the quite limited supply of oxygen and less resident time in the upper region, the CO could not be oxidized to become CO_2 . Therefore, the test runs were carried out at three different EA values: 40%, 60%, and 80%.

Results and Discussion

Temperature Profile

Figure 3 shows the axial temperature profiles along the combustor height for the co-firing of the mixed EB and PNS at $EF_2 = 0, 0.28, 0.53, 0.77,$ and 1 , when firing mixed fuel at EA of approximately 40%, 60%, and 80%. As can be seen in Fig. 3a–c, the EA had significant effects on the average temperature in each co-firing test. By increasing EA at the fixed heat input, the volume of oxidizing air was somewhat higher; therefore, the temperature attained the lower value due to the dilution effect and the heat absorption by the presence of EA .

The secondary fuel energy fraction had a significant impact on the axial temperature. Across the wide range of co-firing tests, the average temperature in the bed region (at $Z = 0.23$ – 0.46 m) was in the range of 750 – 880 °C, while it was approximately 15% lower at 650 – 780 °C in the free-board area. When firing pure PNS ($EF_2 = 1$), the temperature was highest in the main combustion chamber, with its lowest value in the upper chamber. These results could be due to the high density and coarse particles of the PNS; therefore, the fuel was mainly fired at the bottom part of the combustor. Among the other fuel options, mixed fuel with a higher EB proportion had a more uniform temperature profile. The oxidation of fuel/char particles not only occurred in the bed but also in the upper part of the combustor due to the significant carryover of fine particles caused by the lower solid bulk density of the blended fuel. Furthermore, it can also be described by the fixed energy release rate in each test of this experimental procedure.

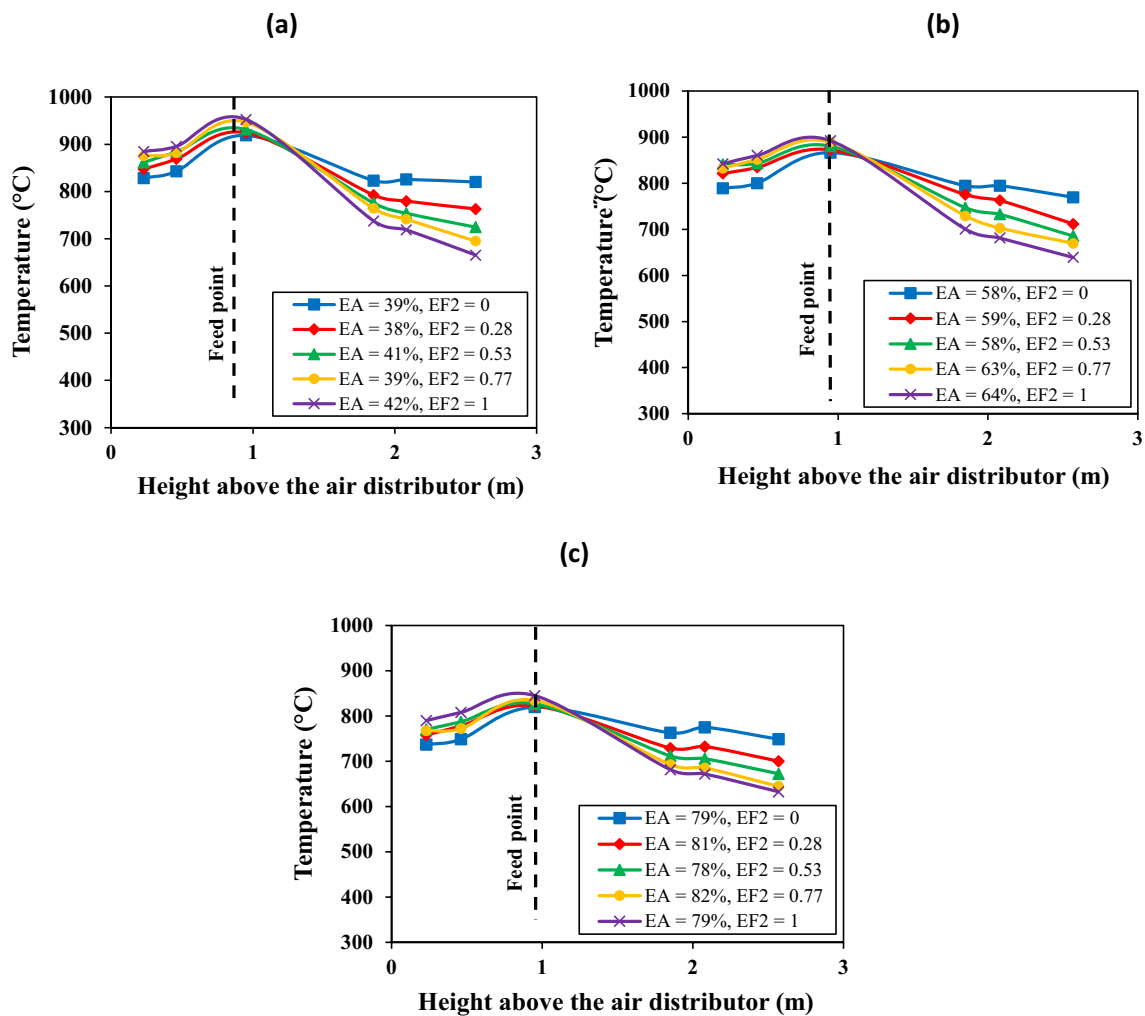


Fig. 3 Temperature profile in TS-FBC for co-firing of mixed EB and PNS at $EF_2=0, 0.28, 0.53, 0.77,$ and 1 with EA of approx. **a** 40%, **b** 60%, and **c** 80%

Local Heat Transfer Coefficient (h_{local})

Figure 4 shows the local heat transfer coefficients at $r/R=0, \pm 1/3, \pm 2/3,$ and ± 1 for the co-firing of the EB (primary fuel) and the PNS (secondary fuel) at $EF_2=0, 0.28, 0.53, 0.77,$ and 1 at $Z=0.46$ m. In the bed splashing zone ($Z=0.46$ m), the radial heat transfer coefficients at the center of the combustor and the combustor wall ($r/R=0$ and ± 1 , respectively) were slightly higher than those at other radial locations of the probe. This phenomenon could be due to the flow pattern of the bed material and the bubble frequency [27]. Using the air distributor's special design, the sand bed was expanded in an upward direction with a swirling movement; therefore, the particles generally rose up in the center and dropped down near the wall. The heat transfer at the center of the combustor was enhanced by the high solid concentration's accelerated interaction frequency (or the rate of renewal) between bed particles and the immersed

surface [34]. Meanwhile, in the area close to the combustor's wall, bubbles frequently occurred due to the strong outward centrifugal force of swirling particles. This increased the turbulence of the flow and the surface renewal frequency rate leading to a slightly higher level of heat transfer. The same behavioral trend was found in the conical FBC studied for gas–solid radial heat transfer using two-dimensional (2D) modeling of the air sand bed [35].

Figure 5 shows the local heat transfer coefficients at $r/R=0, \pm 1/3, \pm 2/3,$ and ± 1 for the co-firing of the EB (primary fuel) and the PNS (secondary fuel) at $EF_2=0, 0.28, 0.53, 0.77,$ and 1 at the TS-FBC's five different heights. In comparison with the splashing or dense bed zone, the local heat transfer in the freeboard region ($Z=2.57$ m) was quite uniform owing to the minimal effects of swirling flow at a very low solid concentration. In this area, gas convection was rather dominant; therefore, the gas behavior's effects on heat transfer were quite obvious.

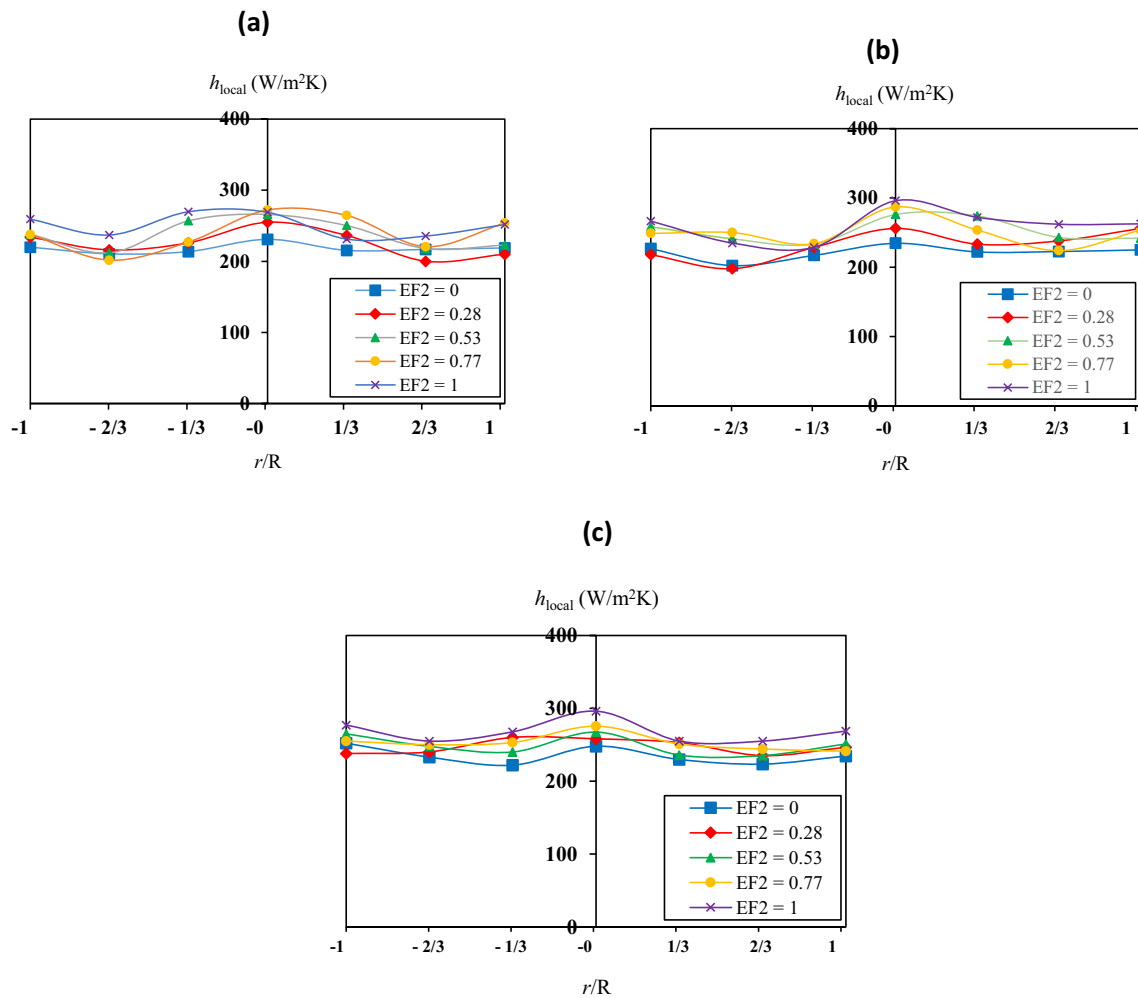


Fig. 4 Local heat transfer coefficient at $Z=0.46$ m in TS-FBC for co-firing of EB and PNS at $EF_2=0, 0.28, 0.53, 0.77,$ and 1 with EA of **a** 40%, **b** 60%, and **c** 80%

Average Heat Transfer Coefficient at Each Combustor Height ($h_{z,avg}$)

Figure 6 shows the effects of EF_2 on the $h_{z,avg}$ in the TS-FBC at EA levels of approximately (a) 40%, (b) 60%, and (c) 80%. The EF_2 noticeably affected the $h_{z,avg}$ in both the dense bed and freeboard regions; however, the $h_{z,avg}$ in the bed region increased at higher EF_2 , whereas the opposite occurred in the freeboard region. Moreover, the EF_2 also demonstrated a significant effect on the location where the maximum $h_{z,avg}$ occurred. As can be seen in the axial profiles in Fig. 6 (c), the highest value of the $h_{z,avg}$ for firing pure EB (at $EF_2=0$) was found at the connecting pipe, while the lowest level was found at the upper part of the combustion chamber for firing pure PNS (at $EF_2=1$). These occurrences could be due to the combustor design. This combustor's connecting pipe was designed to separate coarse fuel particles from fine fuel particles. As the coarse fuel particles and the inert bed

material, due to centrifugal force, fell down to the dense bed zone, a small number of fine fuel particles were expected to escape to the top combustor and fire in this area.

Due to the larger particle size and higher fuel density of the PNS, co-firing of the blended fuel with a higher PNS proportion demonstrated that the vigorous combustion occurred at the bottom part of the combustion chamber. Therefore, the maximum of $h_{z,avg}$ was due to the solid particle convection (sand, fuel, and ash) at the intense heat released rate. With an increasing proportion of the EB, the combustion zone drifted to the higher level as the fine fiber of the shredded EB was easy to ignite and flew to the top of the combustor. When focusing on the hydrodynamics behavior of this fuel option, the upward-swirling flow of hot gas was impeded by a reduced cross-sectional area of the connecting pipe; therefore, the pressure reduced and the hot gas velocity reached the maximum value leading to the highest value of $h_{z,avg}$. From the data analysis when transitioning from firing

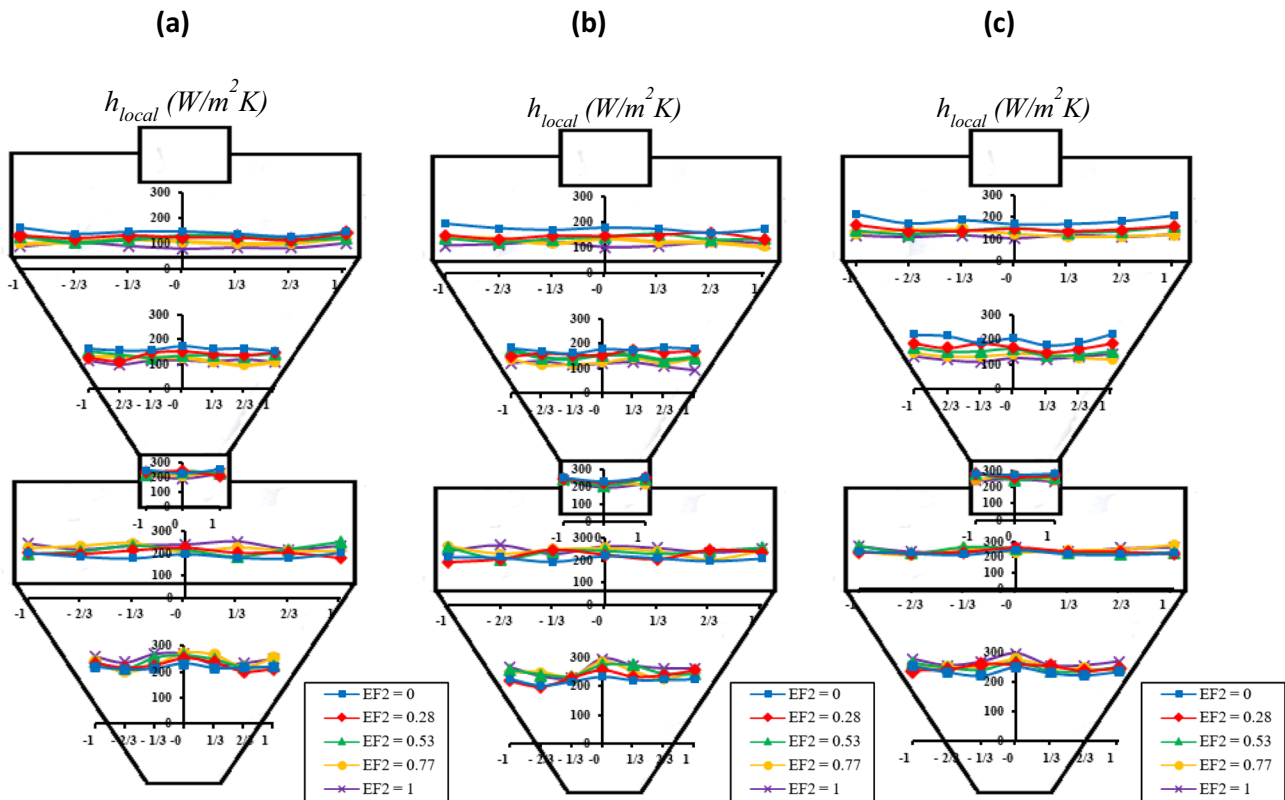


Fig. 5 Local heat transfer coefficient in the TS-FBC for the co-firing of EB and PNS at $EF_2 = 0, 0.28, 0.53, 0.77$ and 1 with EA of **a** 40%, **b** 60%, **c** 80%

pure PNS to pure EB at $EA = 40\%$, it was observed that the $h_{z,avg}$ in the bed region increased from 205 to 242 $W/m^2 K$. Meanwhile, it exhibited the opposite trend in the freeboard region, where the $h_{z,avg}$ in the bed region decreased from 148 to 100 $W/m^2 K$. The same phenomenon was also observed at different EA levels.

Figure 7 shows the effects of EA on the $h_{z,avg}$ in the TS-FBC with three different secondary fuel energy fractions at: (a) 1, (b) 0.28, (c) 0.53, and (d) 0.77. As shown in Fig. 7, EA had significant effects on the $h_{z,avg}$ in both dense bed and freeboard regions. When investigating increases in EA across the scope of this study, the dense bed region appears to provide better mixing and dispersal of bed, ash, and fuel particles, as well as improving particle circulation [25]; therefore, the value of the heat transfer coefficient increased. The higher value heat transfer coefficient could also be due to low heat resistance between the particles and the heat transfer surface at a high gas velocity [36]. In the freeboard region, the heat transfer coefficients also increased in value with the increasing EA ; however, this was a lower level increase due to very dilute solid particles and the process being dominated by gas convection. When increasing EA from 40 to 80% across the wide range of EF_2 values, the $h_{z,avg}$ increased in both the bed and freeboard regions. It

increased from 223 to 246 $W/m^2 K$ (an increase of about 11%) and from 125 to 153 $W/m^2 K$ (an increase of about 22%) in the freeboard region.

For a wide range of operating variables including both EA and EF_2 , the $h_{z,avg}$ in the bed region ranged from 222 to 257 $W/m^2 K$, while in the freeboard area, it varied between 125 and 153 $W/m^2 K$. It can be concluded that the $h_{z,avg}$ in the bed was approximately 40% higher than the freeboard.

Average Heat Transfer Coefficient for Each Operating Condition (h_{avg})

Figure 8 shows the average heat transfer coefficients (h_{avg}) for the various fuel options and the range of EA , with only EA showing significant effects on the h_{avg} . Unlike what is depicted in Fig. 6, where EF_2 shows the significant effects on $h_{z,avg}$ in both bed and freeboard regions. Due to the higher LHV of PNS, the combustor load decreased when increasing EF_2 to maintain the same heat release rate for the blended fuel. Under this condition, the deviation of fuel-ash content should be considered, as it is one of the key parameters in particle heat transfer. As revealed in the literature, heat transfer between cluster particles and the sampling probe could be enhanced by the collision frequency of solid particles of

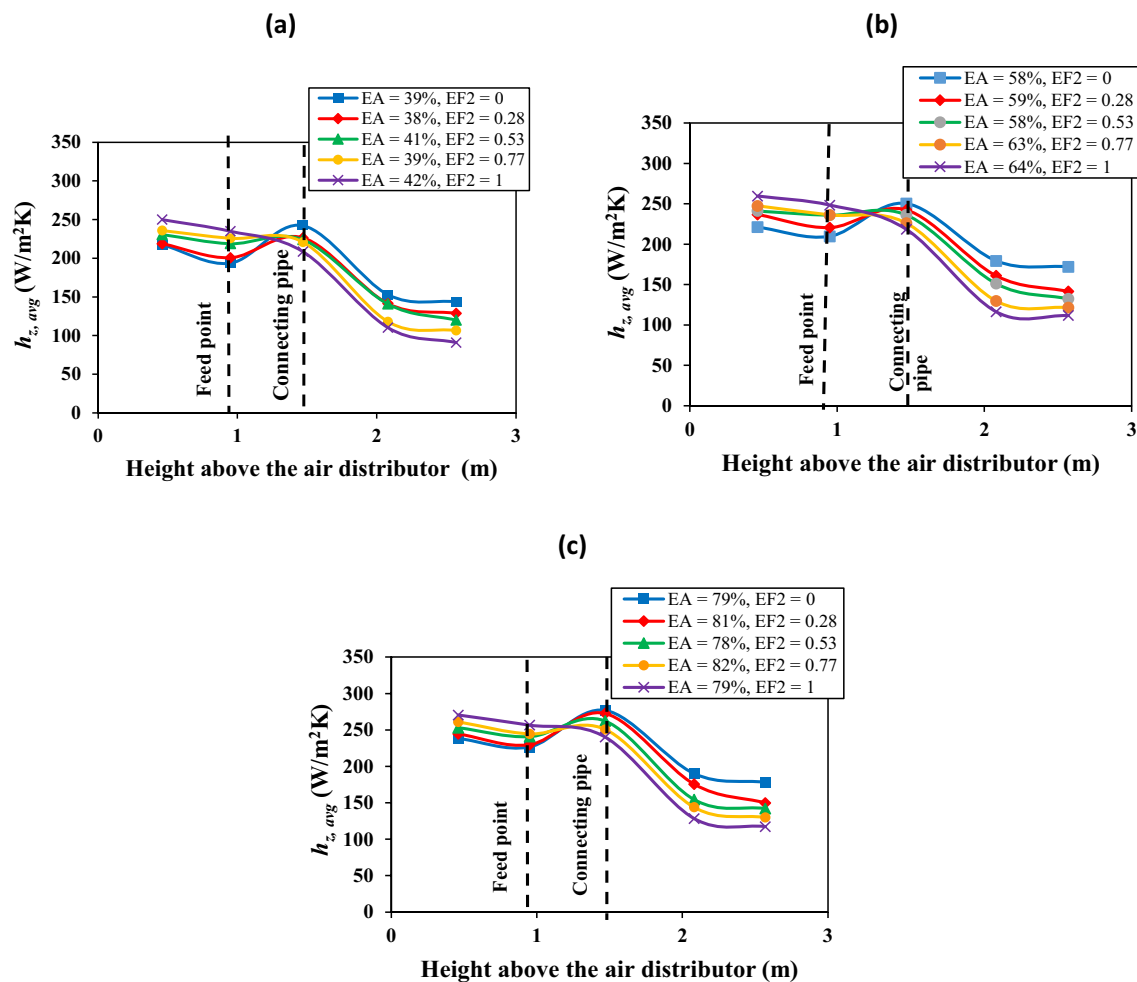


Fig. 6 Effect of energy fraction of secondary fuel on average heat transfer coefficient at each combustor height in TS-FBC at EA of **a** 40%, **b** 60%, and **c** 80%

fuel, ash, and inert bed material in the bed region [32]. However, the fuel properties within the scope of the current study were not found to have significant effects on the h_{avg} , with the reason possibly being the limited area of the sampling probe's heat transfer surface.

The h_{avg} increased with higher EA levels or increasing gas inlet velocity, demonstrating strong agreement with the modeling study conducted by Abdelmotalib and Im [35]. An increase in EA within the fluidized-bed combustor resulted in elevated gas velocity, enhancing the renewal frequency of bed particles and consequently improving gas–particle convection. Due to the low solid density of EB particles, the influence of EA on the h_{avg} was particularly dominant when firing fuel with a higher proportion of EB. By increasing the EA from 40 to 80%, the h_{avg} increased from 170 to 192 W/m² K for $EF_2 = 1$, while it increased from 178 to 205 W/m² K for $EF_2 = 0$. It can be concluded that, across a wide range of EF_2 values, increasing EA from 40 to 80% could result in a 12–15% increase in h_{avg} .

Conclusion

In this study, the heat transfer coefficients were investigated inside a TS-FBC during the co-firing of EB and peanut shell under a wide range of EA and mass fractions of secondary fuel (EF_2). Findings from the study's experimental results are summarized as:

The radial heat transfer coefficients at the center of the combustor and the combustor wall were slightly higher than those in other radial locations by the enhancing of high solid concentration's accelerated interaction frequency between bed particles and the immersed surface.

The average heat transfer coefficient at each combustor height ($h_{z,avg}$) presented the significant effect of both EF_2 and EA. For the wide range of operating variables, the $h_{z,avg}$ in the bed was approximately 40% higher than the freeboard.

When transitioning from firing pure PNS to pure EB at a fixed heat release rate and EA, it was observed that the $h_{z,avg}$

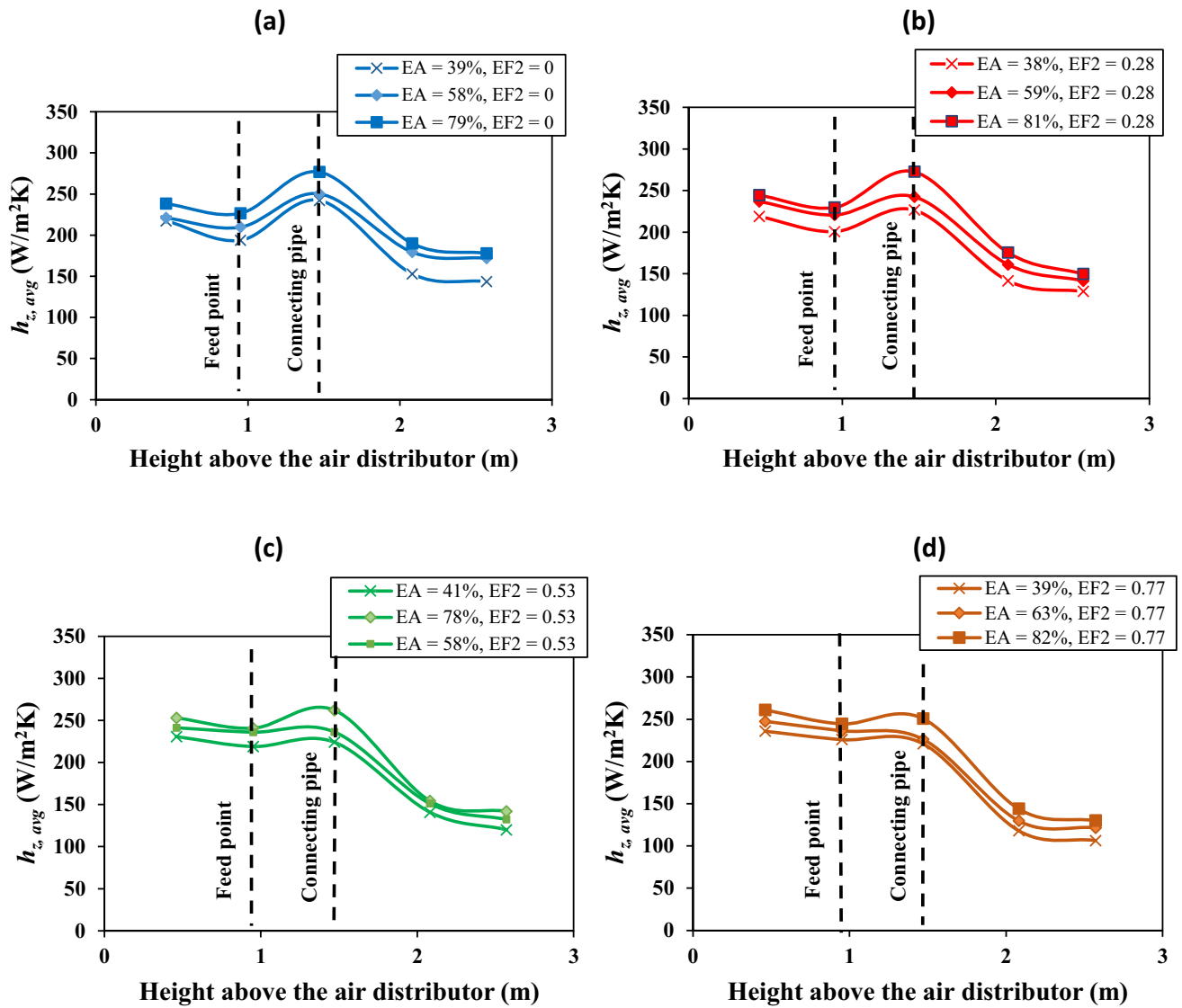


Fig. 7 Effect of EA on average heat transfer coefficient at each combustor height in TS-FBC at energy fraction (EF_2) of a 1, b 0.28, c 0.53, and d 0.77

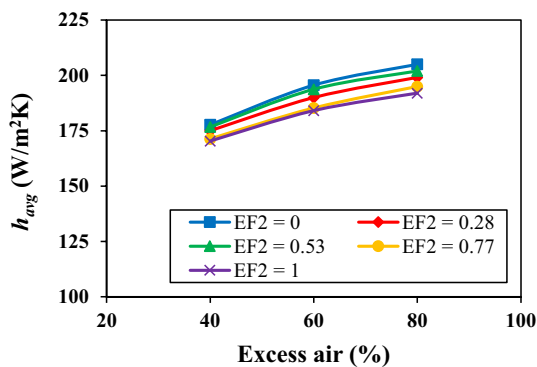


Fig. 8 Average heat transfer coefficient for each operating condition in TS-FBC for wide range of EA and mass fractions of secondary fuel (EF_2)

in the bed region increased, while it exhibited the opposite trend in the freeboard region.

By increasing EA from 40 to 80%, the $h_{z,avg}$ in the bed region could be improved by up to 11%, while it could increase even further, up to 22% in the freeboard region.

In the specified range of operating conditions ($EA = 40\%$ to 80%) with a fixed heat release of 72.5 kW_{th} . The average heat transfer coefficients (h_{avg}) was found in the ranged of 170 to $205 \text{ W/m}^2 \text{ K}$. The EA significant effected on h_{avg} regardless of the value of EF_2 . For a wide range of EF_2 values, the h_{avg} could be increased 12–15% by the increasing EA from 40 to 80%.

Acknowledgements The authors would like to thank all students from the Laboratory of Advanced Combustion Technology and Energy

Systems (LACTES) for their great help with the experimental tests. This research was funded through a grant from the Silpakorn University Research, Innovation and Creative Fund.

References

- European Environment Agency, *2030 Climate Target Plan* (European Environment Agency, Copenhagen, 2021)
- A. Paletto, S. Bernardi, E. Pieratti, F. Teston, M. Romagnoli, *Helvion* **5**, e02070 (2019)
- Department of Alternative Energy Development and Efficiency (DEDE), *Alternative Energy Development Plan 2018–2037 (AEDP 2018–2037)*, Ministry of Energy (MOE), Thailand, https://www.dede.go.th/download/Plan_62/20201021_TIEB_AEDP2018.pdf. Accessed 05 Feb 2023
- M.S. Roni, S. Chowdhury, S. Mamu, M. Marufuzzaman, W. Lein, S. Johnson, *Renew. Sustain. Energy Rev.* **78**, 1089 (2017)
- D. Nordgren, H. Hedman, N. Padban, D. Boströme, M. Öhman, *Fuel Process. Technol.* **105**, 98 (2013)
- V.I. Kuprianov, C. Se, P. Ninduangdee, *Biomass Bioenergy* **127**, 105250 (2019)
- V.I. Kuprianov, P. Arromdee, *Bioresour. Technol.* **140**, 199 (2013)
- K. Sirisomboon, V.I. Kuprianov, *Energy Fuels* **31**, 6856 (2017)
- P. Ninduangdee, P. Arromdee, C. Se, V.I. Kuprianov, *Waste Biomass Valori.* **11**, 5375 (2020)
- Department of Agricultural Extension (DOAE), *Agricultural Production Information System*, Ministry of Agriculture and Cooperatives (MOAC), <http://www.agriinfo.doae.go.th/year63/plant/rotor/perennial/euca.pdf>. Accessed 11 Apr 2023
- G. Almeida, J.O. Brito, P. Perré, *Bioresour. Technol.* **101**, 24 (2010)
- FAO Food and Agriculture Statistics Division (FAOSTAT), *Peanut (Groundnuts with Shell) Production* (Food and Agriculture Organization of the United Nations (FAO), Rome, 2020)
- Department of Agricultural Extension (DOAE), *Agricultural Production Data*, Ministry of Agriculture and Cooperatives (MOAC), <https://www.opsmoac.go.th/jakarta-news-preview-451091791041>. Accessed 11 Apr 2023
- J.G. Woodroof, *Peanuts: production, processing, products* (Avi Publishing Company, Westport, 1983)
- B. Patel, B. Gami, *J. Energy Environ.* **3**, 2 (2012)
- P. Ninduangdee, V.I. Kuprianov, *Biomass Bioenergy* **112**, 73 (2018)
- B. Leckner, *Chem. Mol. Sci. Chem. Eng.* (2016). <https://doi.org/10.1016/B978-0-12-409547-2.12183-3>
- P. Arromdee, K. Sirisomboon, *Eng. J.* (2020). <https://doi.org/10.4186/ej.2021.25.2.207>
- P. Arromdee, V.I. Kuprianov, *Chem. Eng. Process.* **62**, 26 (2012)
- P. Hou, S. MacAdam, Y. Niu, J. Stringer, *Mater. Res.* **7**, 1 (2004)
- Q. Wu, S. Wang, K. Zhang, Y. He, *Appl. Therm. Eng.* **194**, 117128 (2021)
- M.H.M. Tawfik, M.R. Diab, H.M. Abdelmotalib, *Int. J. Therm. Sci.* **147**, 106134 (2020)
- M.F. Mohideen, B. Sreenivasan, S.A. Sulaiman, V.R. Raghavan, *Korean J. Chem. Eng.* **29**, 7 (2012)
- P. Lu, Y. Cao, W.P. Pan, C. Ma, *Exp. Therm Fluid Sci.* **35**, 1127 (2011)
- K. Sirisomboon, P. Laowthong, *Appl. Therm. Eng.* **147**, 718 (2019)
- D. Geldart, A.R. Abrahamsen, *Powder Technol.* **19**, 133 (1973)
- K. Sirisomboon, P. Arromdee, *Powder Technol.* **393**, 734 (2021)
- L. Wang, P. Wu, Y. Zhang, J. Yang, L. Tong, X. Ni, *Appl. Therm. Eng.* **24** (2004)
- J. Sjösten, M.R. Golriz, J.R. Grace, *Int. J. Heat Mass Transf.* **49**, 3800 (2006)
- Y.A. Cengel, A.J. Ghajar, *Heat Mass Transfer: Fundamentals and Applications* (McGraw-Hill Professional, New York, 2014)
- J.P. Holman, *Experimental Methods for Engineers* (McGraw-Hill, Boston, 2001)
- P. Sun, S. Hui, Q. Zhou, H. Tan, Q. Zhao, T. Xu, *Appl. Therm. Eng.* **52**, 284 (2013)
- Pollution Control Department (PCD), *Air Pollution Standards for Industrial Sources* (Ministry of Natural Resources and Environment (MONRE), Thailand, 2013)
- P. García-Triñanes, J. Seville, R. Ansart, H. Benoit, T. Leadbeater, *Chem. Eng. Sci.* **177**, 313 (2017)
- H.M. Abdelmotalib, I.-T. Im, *Int. J. Heat Mass Transf.* **106**, 1335 (2017)
- A.P. Baskakov, B.V. Berg, O.K. Vitt, N.F. Filippovsky, V.A. Kirakosyan, J.M. Goldobin, V.K. Maskaev, *Powder Technol.* **8**, 273 (1973)

Publisher's Note Springer Nature remains neutral with regard to jurisdictional claims in published maps and institutional affiliations.

Springer Nature or its licensor (e.g. a society or other partner) holds exclusive rights to this article under a publishing agreement with the author(s) or other rightsholder(s); author self-archiving of the accepted manuscript version of this article is solely governed by the terms of such publishing agreement and applicable law.